Understanding the Journey of Dopant Copper Ions in Atomically Flat Colloidal Nanocrystals of CdSe Nanoplatelets Using Partial Cation Exchange Reactions

Manoj Sharma[1,2], Murat Olutas[2,3], Aydan Yeltik[2], Yusuf Kelestemur[2], Ashma Sharma[1,2], Savas Delikanli[1,2], Burak Guzelturk[2], Kivanc Gungor[2], James R. McBride[4], and Hilmi Volkan Demir [1,2]*

[1]LUMINOUS! Center of Excellence for Semiconductor Lighting and Displays, School of Electrical and Electronics Engineering, School of Physical and Mathematical Sciences, School of Materials Science and Engineering, Nanyang Technological University, Nanyang Avenue 639798, Singapore.

[2]Department of Electrical and Electronics Engineering, Department of Physics, and UNAM–Institute of Materials Science and Nanotechnology, Bilkent University, Ankara 06800, Turkey.

[3] Department of Physics, Abant Izzet Baysal University, Bolu 14030, Turkey.

[4]Department of Chemistry and Vanderbilt Institute for Nanoscale Science and Engineering, Vanderbilt University, Nashville, Tennessee 37235, United States.

*Corresponding Author:

Email: volkan@stanfordalumni.org, hvdemir@ntu.edu.sg

Unique electronic and optical properties of doped semiconductor nanocrystals (NCs) have widely stimulated a great deal of interest to explore new effective synthesis routes to achieve controlled doping for highly efficient materials. In this work, we show copper doping via post-synthesis partial cation exchange (CE) in atomically-flat colloidal semiconductor nanoplatelets (NPLs). Here chemical reactivity of different dopant precursors, reaction kinetics and shape of seed NPLs were extensively elaborated for successful doping and efficient emission. Dopant-induced Stokes-shifted and tunable photoluminescence emission (640 to 830 nm) was observed in these Cu-doped CdSe NPLs using different thicknesses and heterostructures. High quantum yields (reaching 63%) accompanied by high absorption cross-sections (>2.5 times) were obtained in such NPLs compared to those of Cu-doped CdSe colloidal quantum dots (CQDs). Systematic tuning of the doping level in these two-dimensional NPLs provides an insightful understanding of the chemical dopant based orbital hybridization in NCs. The unique combination of doping via partial CE method and precise control of quantum confinement in such atomically flat NPLs originating from their magic-sized vertical thickness exhibits an excellent model platform for studying photo-physics of doped quantum confined systems.

Doping of transition metal ions into semiconductor colloidal quantum dots (CQDs) enables exciting electronic and optical properties.[1–6] In the past two decades, a lot of attention has been given to explore the new synthesis methods for the electronic doping of CQDs to understand the resulting novel properties and to use them in optoelectronic applications.[2–4,7–10] With this overarching goal, different synthesis methods have been developed for the preparation of such doped nanomaterials from the molecular precursors.[11] These direct

synthesis methods require a careful control of nucleation, growth and surface chemistry for achieving the desired morphology and a different range of optical to electronic properties.[12–15]

On the other hand, cation exchange (CE) has emerged as a simple and versatile tool for the synthesis of different nanomaterials, which are otherwise difficult to synthesize through other conventional synthetic routes.[16,17] CE reactions allow for the necessary post-synthesis modifications of the pre-synthesized nanocrystals (NCs) into stepwise-controlled new complex nanomaterials.[16–19] Accompanied by the success of full CE method for obtaining new nanomaterials from existing pre-synthesized NC seeds, in the recent years, partial CE method has been a favorable alternative for the doping of semiconductor CQDs.[2,20] In partial CE reactions, a few of the dopant cations are replaced by the host cation in the crystal lattice leading to interesting electronic, optical, and magnetic properties.[2,20] Using the partial CE reactions at room- and moderately high-temperatures, successful doping has been shown for binary (e.g., CdSe, ZnSe)[2,3] and ternary (e.g., CuInS, ZnInS)[21] semiconductor CQDs.

In particular, the Cu(I) doping of CdSe CQDs has been shown via heat-up methods and, more recently, by a high-temperature CE method.[3,10] As such, successful doping at the substitutional sites has resulted in Cu(I)-related emission. Increased Cu(I) ion doping in CdSe CQDs synthesized through heat-up methods exhibit red-shifting dopant emission spectra.[22] Using theoretical and experimental methods, it has been shown that orbital hybridization between the chemical dopant and the host cation (Cd) results in a shift of the conduction band (CB) edge only, which in turn red-shifts the Cu(I) emission with the enhancement in the doping concentrations.[22] However, it is difficult to control the size of NCs at different doping levels, which interferes with the orbital hybridization induced red-shift in the photoluminescence (PL) emission spectra. Partial CE method allows to use the same core for

adding different amounts of chemical dopants. Such pre-synthesized cores having exactly the same size distribution can serve as an excellent host for comparing the PL emission spectra of differently doped quantum confined systems. Sahu et al. previously reported on doping different amounts of silver (Ag) in CdSe CQDs,[2] and later the doping of Cu and Ag in CQDs was also reported by using a similar aforementioned partial CE reactions.[20] However, in none of these studies efficient dopant induced emission was found.

Atomically flat NCs, also known as colloidal nanoplatelets (NPLs), or alternatively as "colloidal quantum wells" (CQWs), have attracted great interest in the past few years among all colloids thanks to their strong 1D confinement along with their magic-sized vertical thicknesses and assorted heterostructures (core-crown, core/shell, core/crown/shell)).[23–25] As compared to the CQDs, this new class of NCs features superior optical properties including narrow spontaneous emission spectra, suppressed inhomogeneous emission broadening, extremely large linear and nonlinear absorption cross-sections[26,27] and giant oscillator strengths.[28,29] Recently, using full CE methods, core only CdSe NPLs have been shown to be converted into $Cu_{2-x}Se$ and HgSe NPLs.[30,31] In addition to the core only NPLs, CdSe/CdS core/shell NPLs have been also successfully converted into Cu_2Se/Cu_2S, ZnSe/ZnS and PbSe/PbS NPLs.[19] However, unlike CQDs, there is no systematic study for electronic doping of these CQWs using partial CE reactions. Furthermore, the observation of pure vertical confinement in these atomically flat CQWs makes them a highly appealing model host system for studying variable doping effects without considering variation in the quantum confinement effect.

Very recently, we have shown successful Cu(I) doping in 3-4 ML of CdSe NPLs using a high-temperature nucleation doping method.[32] These doped NPLs have shown large Stokes-shifted dopant-induced emission in red to near-infrared (NIR) regions of the electromagnetic spectrum with high quantum yields (~97%). Furthermore, they were

successfully shown to be applied as luminescent solar concentrators (LSCs) for harvesting solar light. However, limited control over the doping level with the nucleation doping method makes it practically impossible to understand the doping mechanism and the origin of this efficient dopant emission from these vertically magic-sized NPLs (e.g., ~1.2 nm for 4 ML CdSe). Therefore, we hypothesized that partial CE reactions can serve as a convenient method enabling the precise control of the doping level and its resulting excitonic features by using precursor reactivity, time and temperature of reactions. Furthermore, doping of Cu(I) into NPLs having different thicknesses and heterostructures (e.g., 5 ML CdSe, and core/shell NPLs) could possibly be achieved with the CE method to further tune their highly desired excitonic features.

Here, we propose and develop the Cu-doped CdSe NPLs via the post-synthesis partial CE method. In this work, we carried out a systematic and detailed study to understand the effect of doping into these NPLs with the use of slowly varying amounts of Cu(I) ions. Various techniques including inductively coupled plasma mass spectroscopy (ICP-MS), high-angle annular dark-field (HAADF) scanning transmission electron microscopy (STEM) combined with energy-dispersive X-ray spectroscopy (EDS) mapping and X-ray photoelectron spectroscopy (XPS) have been used for the confirmation of Cu(I) doping. With the doping of core-only NPLs having different thicknesses (3-5 ML), we achieved tunable dopant-induced emission covering a wide range of the electromagnetic spectrum from the visible to NIR. The combined analyses of these results from the excitation-dependent steady-state PL spectroscopy and high-resolution XPS depth profile have demonstrated successful doping of Cu(I) ions in the host medium of the CdSe NPLs, and this is responsible for the dominant and strong dopant-related tunable PL emission with reduced self-absorption and high PL quantum efficiencies reaching 63%. By controlling kinetics of the partial CE, we studied the journey of Cu ions from the interstitial to the deep substitutional sites.[16]

Intentional slow doping via partial CE reactions has allowed us to understand chemical dopant induced orbital hybridization of the host cadmium (Cd) ions. Furthermore, the underlying mechanism of this efficient dopant-induced PL emission has been investigated and understood by using temperature-dependent time-resolved fluorescence (TRF) spectroscopy.

Results and Analyses

Using the partial CE method, the atomically flat CdSe NPLs having different vertical thicknesses (e.g., 3-5 MLs) have been doped with Cu(I) ions (Figure 1a). First, we synthesized the 4 ML thick undoped core-only CdSe NPLs having a zinc-blende crystal structure with earlier reported recipe.[23,24] These NPLs were used for the synthesis of Cu-doped CdSe NPLs with varying Cu(I) concentrations. It has been recently reported that CdSe NPLs can be rapidly converted into $Cu_{2-x}Se$ NPLs because the d-spacing of bulk CdSe and bulk $Cu_{2-x}Se$ differ by only 5-6%, which enhances the CE with Cu(I).[16,30] In our study, to avoid the full CE, we used trioctylphosphine (TOP) as the surfactant to controllably mediate the incorporation of Cu(I) ions into the CdSe NPLs as the dopant (see methods section for the detailed information). Briefly, variable amounts of ethanolic solutions of $Cu(OAc)_2$ and $Cu(NO_3)_2$ premixed with TOP were added to the known concentrations of undoped 4 ML CdSe NPLs under stirring in nitrogen-filled glove box at 50 °C (Figure 1a). The partial CE reaction was completed after 1 h with the addition of ethanol and repeated washing of the NPL samples. Finally, all the samples were dispersed in toluene and kept on stirring for 1-9 days at 50 °C under ambient conditions. Various optical measurements were performed every day to understand the evolution of dopant emission and reactivity of different dopant precursors.

Figure 1b depicts the UV-visible absorption and steady-state PL spectroscopy results for the undoped and 0.9% Cu-doped 4 ML CdSe NPLs (as an exemplary case). In the

absorption spectrum, both electron-heavy hole (e-hh) and electron-light hole (e-lh) transitions for the doped NPLs stay unchanged, suggesting that 0.9% Cu(I) doping does not alter the discrete excitonic features of the NPLs. The normalized PL emission spectrum for the undoped CdSe NPL exhibits a spectrally narrow emission peak at ~513 nm having a full-width at half-maximum (FWHM) of ~10 nm, which is characteristic to the CdSe NPLs having 4 ML vertical thickness.[24] For the doped-NPLs, a large Stokes-shifted broad emission at a higher wavelength region (>650 nm) is observed in addition to the band-edge (BE) emission at ~513 nm. Herein, origin of the broad and Stokes-shifted emission appears to be similar to Cu(I) doped CdSe CQDs.[33,34] Briefly, this kind of broadband emission has been observed to originate from the recombination of delocalized electrons in the CB with strongly localized holes in Cu(I) states and is referred to as metal-to-ligand (conduction-band) charge transfer ($ML_{CB}CT$) emission. Therefore, the mid-bandgap position of Cu(I) dopant ions results in the Stokes-shifted emission.

To deeply understand the emission profiles of all these doped and undoped NPLs, time-resolved fluorescence spectroscopy (TRF) using a time-correlated single photon counting system (TCSPC) was utilized. In the undoped NPL ensemble, a broad defect emission was observed (Figure 1b). The fluorescence decay curve of this defect emission is shown in Figure 1c, in which the decay was also compared to that of the dopant-related emission in the doped NPL ensembles. There is a stark contrast between the decay curves, which indicates that the large Stokes-shifted emission in the doped ensemble is not due to the surface trap states but originates from the excited state between the CB of the CdSe NPL and the localized hole state of the Cu dopant. This observation is consistent with the previous literature on the Cu-doped NCs.[1,34–38] Average lifetimes for the dopant emission are 512 and 480 ns for acetate and nitrate precursor based samples, respectively, whereas average lifetime of defect emission from the undoped NPLs is 180 ns. Indeed, the PL lifetime of the transition

metal ions such as Mn and Cu is very long as stated in the previous reports for CQDs.[4,34,37,39] This implies that the Cu(I)-related emission in NPLs appears similar in nature with 3D confined CQDs.

For the systematic investigation of this large Stokes-shifted emission in the doped NPLs and the variation in the contribution of BE to the dopant-related emissions, we synthesized a wide range of Cu(I)-doped CdSe NPLs by increasing both acetate and nitrate precursors in the partial CE reactions. Copper to cadmium ratios (i.e., Cu(I):Cd(II)) were obtained for all the samples via ICP:MS measurements. To this end, all the doped samples were washed extensively with ethanol before the ICP measurements to remove any un-reacted Cu(I) ions or excess Cd ions on the NPL surface. Figures 2(a-c) and 2(d-f) depict the results and their analyses from the UV-visible absorption and steady-state PL spectroscopies for the undoped and Cu(I)-doped 4 ML CdSe NPLs using acetate and nitrate based copper precursors, respectively. Absorption spectra for all samples using acetate precursors suggest e-hh and e-lh transitions remained unaffected at all studied doping levels. On the other hand, consistent increase in the nitrate precursors leads to degradation of excitonic features of the NPLs (see Figure 2d and Figure S1). In the absorption spectra for the doped samples, there exists a weak tail along with e-hh transition (at the lower photon energy) as compared to the undoped NPLs (Figures 2a and 2d), which is attributed to the metal-to-ligand (conduction band) charge transfer ($ML_{CB}CT$) absorption state for the Cu-doped CdSe CQDs.[3,36]

Figures 2b and 2e show the PL emission spectra of Cu (0-3.6%) and Cu (0-2.2%) doped NPLs with the use of copper-acetate and -nitrate precursors, respectively. For the both cases, increase in the Cu-doping results in an increase in the dopant-related Stokes-shift of the emission with respect to the BE emission. However, the variation in relative intensities between the BE and dopant-related emissions as a function of the Cu(I) concentration in the doped NPLs seems more complex than similarly doped CdSe CQDs studied in the related

literature.[3,34,35] To follow these variations, we summarized useful information from the emission spectra for both the series given in Figures 2c and 2f. Concisely, this summary illustrates that the fraction of total integrated PL intensity associated with the $ML_{CB}CT$ emission (I_{dopant}/I_{tot}) and its peak emission wavelength changes with the increase of Cu(I): Cd(II) ratio in the CdSe NPL host medium. In Figure 2c, the emission contribution coming from dopant ions (Cu^+ PL fraction) becomes monotonically stronger as the Cu^+ concentration is increased up to the value of 1.7%. For Cu(I) concentration of 1.7%, the dopant emission has the highest overall contribution (97.8%). For the higher Cu(I) concentrations above 1.7%, the BE emission starts to recover again and, hence, the dopant emission contribution starts to decrease. Interestingly, the PL peak emission wavelength for the dopant-related emission also redshifts in a monotonic manner with the increasing dopant concentrations up to 1.7%. Thereafter, it follows dopant emission contributions and starts to blueshift.

We also performed PL excitation (PLE) measurements to find out the origin of the large Stokes-shifted PL emission in the doped NPLs. Figure S2 shows the excitation spectra of the Cu-doped NPLs with varying Cu concentrations (0.9, 1.7 and 3.2%). The excitation spectrum of the large Stokes-shifted PL emission essentially resembles the absorption spectrum of the doped NPLs (see Figure 2a), which indicates that the large Stokes-shifted emission originates from the doped NPLs. Further, the PL excitation spectra measured for different spectral positions of the longer-wavelength emission peak (i.e., at the peak, red- and blue-tails), do not show any discernible spectral difference (see Figure S3). It suggests that there is no inhomogeneous broadening in the doped NPLs thanks to their magic-sized vertical thicknesses.

In the case of doping with nitrate precursors, almost complete dopant emission appears at the 1.2% Cu(I) doping levels (Figures 2e and 2f). Thereafter, further increase in doping percentage results in slight decrease of dopant contribution in the PL emission

spectrum. Consistently, the PL peak emission wavelength in this case also follows the same trend. Here, contrary to the cases of acetate precursor shown in Figure 2b, almost full dopant emission emerges at 1.2% of Cu(I) doping. This suggests that the use of different precursors affect the emission dynamics. The different reactivity of both precursors might affect distribution and nature (interstitial/substitutional) of the doping in these atomically-flat NPLs.

Contribution of the BE emission in the doped NPL ensembles can be explained by two different hypotheses. The first is that all of the NPLs are doped and the BE emission appears from the doped NPLs, which has been shown for the Cu(II) doping in the NCs.[6] This previous report suggests Cu existing in +2 oxidation state creates "persisting holes", which can allow for the BE recombination competing with Cu(II)-related recombination. However, most of the research suggests the second hypothesis that Cu is doped as the +1 oxidation in CdSe CQDs, upon photo-excitation which converts to the +2 state, resulting in a dominant Stokes-shifted dopant emission.[3,33,40,41] Therefore, Cu having the +1 oxidation state in CdSe CQDs cannot fundamentally allow any BE emission in the Cu(I)-doped NCs. The only possibility for co-appearance of the BE and dopant emissions can result from two different sub-populations within the doped ensemble: doped and undoped NCs. This second hypothesis has been recently verified via single-particle measurements for 0.6% Cu(I)-doped CdSe CQDs.[34] However, in our case, apart from the undoped sub-population, uneven distribution of dopant ions among individual NPLs may also result in the BE emission. Since, the lateral dimension of these 4 ML NPL (14.0 ± 1.5 nm × 12.9 ± 1.9 nm) is large in comparison with previously studied Cu(I): CdSe CQDs (~3.5 nm). Moreover, due to different reactivity of the acetate and nitrate precursors during partial CE reactions, there is a possibility of different doping distribution among individual NPLs. As seen from Figures 2c and 2f, at similar doping levels (0.9%), nitrate precursor based doped NPLs show nearly full dopant emission contribution (99.4%) as compared to acetate precursor based doped NPLs (96.7%). This

suggests nitrate precursor reacts faster in the CE reactions as compared to acetate ones, or in other terms they provide more uniform distribution of Cu(I) dopant ions among CdSe NPLs. Furthermore, the appearance of BE emission at higher doping values (e.g., > 1.7%, see Figure 2b) decreases the probability of sub-populations. Therefore, further investigations are needed for understanding the emission mechanism for these newly studied Cu-doped NPLs.

Structural and elemental investigations were also conducted to verify the Cu(I) doping and its distribution among the NPLs studied in this work. High-angle annular dark-field transmission electron microscopy (HAADF-TEM) images of the undoped and Cu-doped CdSe NPLs (for the exemplary cases of 1.7 and 1.2% Cu(I)-doped samples from acetate- and nitrate-based samples) present regular rectangular shapes with average lateral dimensions of 14.0 ± 1.5 nm by 12.9 ± 1.9 nm and a vertical thickness of 1.2 nm corresponding to 4 ML of CdSe (Figures 3a-3c). Here it was observed that there is no significant change in the lateral size distribution of NPLs (see also Figures S4a and S4b)) and their crystallinity after the Cu-doping process (compare to high-resolution bright-field TEM images of the undoped, 1.7% Cu(I)-doped NPLs in Figures S5a and S5b). Figure S6 exhibits the XRD pattern acquired from the undoped and doped NPLs and shows their characteristic peaks arising from the zinc-blende structure. In the doped samples, structural features do not change as compared to the undoped samples, which has been also observed in the selected area electron diffraction (SAED) pattern as shown in the inset of Figures 3a-3c.

The presence of copper ions in the host CdSe NPLs has been confirmed through HAADF-STEM microscopy with individual energy dispersive spectroscopy (EDS) maps for cadmium (Cd), selenium (Se) and copper (Cu). Figure 3d shows the HAADF image of 3.6% Cu-doped NPLs. For the selected group of NPLs shown in Figure 3d, individual elemental maps are presented in Figures 3e-3g. Figure 3h shows the overlaid EDS map of Cd and Cu. Even at very low doping levels, we can explicitly observe the presence of Cu ions in the

NPLs along with Cd and Se. However, considering the instrumental limits the identification of the exact location and distribution of Cu dopant ions in NPLs is practically not possible. At the same time, the HAAD-STEM microscopy with individual EDS maps along with EDS spectra still provide useful information by confirming successful Cu doping in CdSe NPLs (Figures 3e-3g and Figures S7-S11).

To further verify the Cu-doping in the NPLs, we employed XPS measurements, the results of which also prove the successful doping in the NPLs. Apart from showing the presence of Cu in the NPLs, XPS additionally provides insight about the possible oxidation states for these dopant ions. For the analysis, all of the peaks have been spectrally corrected according to carbon 1s standard peak. Figure 3i shows the high-resolution XPS spectra of 3.6% Cu-doped NPLs for Cu 2p-orbitals. We find Cu 2p-peaks at 932.55 and 955.35 eV corresponding to $2p_{1/2}$ and $2p_{3/2}$ orbitals, respectively.[30,37,42] Spin-orbital splitting of Cu(I) ions in our case is 19.8 eV, which is in good agreement with the reported value of 19.6 eV in the literature.[10,37] Moreover, the absence of any satellite peaks strongly suggests the absence of Cu(II) in our doped NPLs.[37,42] Therefore, these well screened peaks in our spectra indicate the presence of either Cu(I) or Cu(0) oxidation state in the CdSe NPLs. The Auger Cu LMM spectrum further offers that the valence state of Cu in the NPLs should be 1+ (see the inset of Figure 3i), which is in accordance with the recent literature of Cu(I) doped CdSe CQDs.[16,22,36]Additional XPS analysis, survey-spectrum and high-resolution XPS for Cd and Se are provided in Figure S12-S13.

Different elemental characterizations apparently evidence the presence of Cu(I) dopant ions in the host CdSe NPLs. However, it is difficult to see the doping distribution among these atomically flat individual NPLs. Therefore, to understand doping distribution and BE to dopant-related emission contribution among individual NPLs, we carried out additional experiments by carefully varying the reaction time of partial CE process, doping

concentration, initial PL quantum yield of the cores, and by using different lateral sized control groups of undoped NPLs. Detailed optical characterizations were conducted on every day to understand evolution of dopant-related PL emission and the emission dynamics (Figures 4a-4f and Figures S14-S17). It is worth mentioning that, to compare the dopant-related emission among different 4 ML samples, we performed these partial CE reactions under exactly identical conditions. For example, all undoped 4 ML cores possess exactly the same optical density and their partial CE reactions were followed by addition of the same amount of $Cu(OAc)_2$ precursors. Therefore, results presented in Figure 4 can be compared among themselves. However, additional analyses with the use of $Cu(NO_3)_2$ precursors are also provided in the supporting information (Figure S17). Furthermore, in order to understand the kinetics of these partial CE reactions during first 1 h we measured steady-state PL emission at different time periods (Figure S18). PL emission spectra show very little difference in the dopant emission contribution during first 1 h of the reaction.

Figures 4a-4c present the UV-visible absorption, PL emission and PL decay curves of the Cu-doped NPLs exposed to stir for 1, 5 and 9 days after the partial CE reactions. Detailed analysis for each day is given in Figure 4d. As shown in Figure 4a, on day 1, immediately after completion of the partial CE, all excitonic absorption features remain intact. In the PL emission spectra (shown by blue solid line in Figure 4b), dopant-related Stokes-shifted emission can be seen along with the dominant BE emission. However, the PL emission contribution of this dopant emission with respect to the total emission is weak. As discussed above, these doped samples were kept under stirring continuously. With the passage of time during stirring, the dopant emission starts to appear. Particularly, for the day 5 measurements, the emergence of almost complete dopant emission could be observed with slight red shift in its peak wavelength. However, recovery of some BE emission with slight blue shift of this dopant emission was observed on day 9 (shown by red solid line in Figure 4b). Moreover,

slight increase in the absorption spectra (at > 800 nm) was found for the samples measured on day 9 (see the inset of Figure 4a). The PL decay curves for this dopant emission peak on day 1, 5 and 9 are shown in Figure 4c. It is clearly seen from the inset of Figure 4c that the presence of the fast decay component along with a long dopant-related one. With the passage of time, for the fifth day measurement, the complete elimination of this fast trap-related PL decay component was observed. These TRF measurements explicitly support the evolution of the dopant-related emission dominating over time. The evolution of Cu(I) emission fraction, change in the emission peak wavelength and QY values are summed up in Figure 4d.

These results point out that, with time, the doped Cu(I) ions in CdSe lattice, which may be located on surface or interstitial positions, get incorporated into deep substitutional positions. Cu(I) doping into CdSe CQDs has been described in the literature by a two-step process starting from interstitial to deep substitutional doping.[10,16,22] Therefore, intentional slowing of the partial CE doping by using less reactive acetate-based precursor may allow for our understanding of the evolution of this Stokes-shifted emission. As shown in Figure 4d with the passage of time, both dopant emission based PL fraction and QY of sample increases which supports the transfer of the interstitial/surface present Cu(I) ions into the deep substitutional sites. Furthermore, the red shift in Cu(I) emission peak is also synchronous with the trends of dopant emission fraction contribution and QY results. Recently, similar red shift in the PL emission spectra for Cu(I) doped CdSe CQDs has been shown with the increase in substitutional doping of Cu-ions.[22] Their theoretical and experimental studies show the increase in Cu(I) doping results in orbital hybridization of lower CB states, which leads to red shift in the PL emission spectra. The slow increase in Cu emission for acetate based samples with the prolonged time of stirring after the completion of partial CE can also be possibly explained with the increase in Cu doping amounts in NPLs by unreacted Cu ions present in the solution or surface of NPLs. In order to understand this possibility, after the

completion of partial CE for 1 h in the glove box, we divided the whole sample into two parts and cleaned them 2 times and 5 times respectively with ethanol. Thereafter, they were allowed to stir under ambient at 50°C continuously for 1-10 days. As shown in PL spectra on the final day the Cu PL fraction appears to be nearly similar in both of the cases (Figure S19). On purpose we normalized both of the PL spectra at their band-edge peaks. Therefore, we can compare the emergence of Cu PL emission for both the cases. We believe that after 5 cleanings any unreacted Cu precursor present in the solution or surface should be cleaned and only doped NPLs should precipitate. However, both 2- and 5- cleaned samples show almost similar Cu emission contribution. Furthermore, in both the cases, the peak position of Cu emission is also similar, which suggests the same degree of hybridization or nearly similar Cu doping percentage for both the cases. This result indirectly suggests that it is less likely for any unreacted Cu to be present in the solution. Therefore, slow rise in the dopant emission for the case of copper acetate precursor is attributed to the slow diffusion of surface/interstitial dopant ions into substitutional sites, which result in an efficient dopant emission. Therefore, our detailed optical studies show possible deep substitution of the doping Cu(I) ions in CdSe NPLs.

As seen in Figure 4d, initial PL QY of the undoped core-only NPLs having 170.3 nm^2 lateral area was measured as 32.0%, whereas the highest PL QY achieved for the same NPL ensembles with the given amount of added Cu precursor is 33.8%. In order to comprehend the role of initial PL QY of undoped core-only NPLs for the partial CE process, we cleaned the same undoped-core four times with ethanol to remove surface ligands. As expected, the removal of ligands results in a significant decrease in the PL QY of the core-only undoped NPLs. Therefore, partial CE reactions with the same sample possessing 4.5% initial QY were conducted under identical conditions. Figure 4e depicts the steady-state PL emission measurements for these experiments. Interestingly, the highest PL QY for this sample was

found to be 35.3% which is very similar to the sample shown in Figure 4d. However, this poor initial PL QY sample takes 6 days to reach full Cu(I) PL fraction and the highest PL QY (Figure 4e). Briefly, the partial CE on both samples shows that initial QY of the undoped cores does not affect the final quality of doped samples. Therefore, only successful Cu(I) doping results in high QY for these doped samples.

Next, we studied 4 ML undoped core NPLs having large lateral area (i.e., 366.6 nm^2) under identical experimental conditions. Figure 4f shows the evolution of Cu(I) PL fraction with time and the variation of its peak wavelength along with the corresponding PL QY measurement on each day. The results indicate that the same amounts of Cu(I) dopant addition lead to almost the same final PL QY of the doped samples. However, the large lateral area of such undoped cores delay the appearance of complete dopant emission and hence achieving the highest PL QY. Clearly, the controlled emergence of dopant emission in these large starting cores as such with this partial CE method allows to understand doping mechanism in these strongly quantum confined NCs. The detailed UV-visible absorption, steady-state PL emission spectrum and PL QY values each day for all the samples discussed in Figures 4d-4f are presented in the supporting information (Figures S14-S16).

The recovery of BE emission with the delayed stirring (≥7 days), decreased PL QYs, and consistent blueshifting of the dopant-related emission peak collectively suggest the overall decrease of Cu(I) doping at the substitutional sites (see Figures 4b and 4d-4f). At the same time, conversion of Cu-doped CdSe to Cu_2Se (fully or partially) may result in this blueshifting of PL emission spectrum along with the recovery of BE emission and overall decrease in the PL QYs. Moreover, slight increase in absorption (at >800 nm) was also observed for almost all samples from day 7 onward (Figure 4a and Figures S14-S16). Similar observation for the appearance of Cu_2Se-related absorption by conversion of Cu-doped CdSe to Cu_2Se has been previously reported by Gamelin et al. for CQDs.[3] However, these partial

CE reactions can be stopped at any desired point and hence preserve the desired PL emission spectra. These samples were found to be stable for over one year under ambient conditions. Earlier, as compared to CdSe CQDs, Au decorated CdSe NPLs and CdSe to $Cu_{2-x}Se$ converted NPLs were shown to be resistant to oxidation.[30,43,44] In the literature, formation of oxides on these CdSe surface is studied by Se 3d core level high- resolution XPS spectra where the SeO_2 peak at 58.8 eV clearly shows the oxidation of CdSe NCs. Furthermore Cd 3d spectra is also used to indicate the possible oxidation of NCs.[44] They observed broadening of Cd 3d after oxidation of CdSe NCs. In our case for different samples we did not observe any SeO_2 peak in high-resolution XPS spectra of Se 3d orbitals (Figures S12-S13). Furthermore, there is no indication of oxidized Cd 3d peaks in the high-resolution XPS spectra for all our doped and undoped samples stored over long time in ambient.

Here among different series of doped-NPLs synthesized by the same partial CE method, we obtained the highest PL QY to be around 63%. To achieve the dominant and efficient dopant emission quickly through these partial CE reactions, we investigated the effect of temperature. Surprisingly, annealing of the doped-NPL ensembles in the solution-state shows the transformation of doped-NPLs emitting both BE and Cu(I) emission to only Cu(I)-related emission. Moreover, this shift results in increase of the PL QY of doped samples. Figures 5a-5d depicts UV-visible absorption and PL emission spectra for two samples before and after annealing process. Consistently, both samples show annealing at 120 °C under N_2 for 30 min, which leads to successful elimination of the BE emission and then the successful Cu(I) emission with very high PL QYs. We observed that after annealing the PL QY increases from 21% to 44% and 28% to 51% for the cases of acetate- and nitrate-based samples, respectively. Time-resolved fluorescence measurements before and after the annealing indicate that the PL decay curves slow down, suggesting the suppression of the competing nonradiative channels (see Figure S21 and Table S1). Moreover, conversion of

doped NPLs emitting from the band-edge and dopant emission to only dominant dopant emission and red-shift of dopant peak supports our earlier presented emission mechanism. Briefly, annealing of the samples synthesized using copper acetate precursor shows larger red-shift (692-764 nm) as compared to doped NPLs synthesized by using nitrate precursor (728-758 nm). As discussed previously, the red-shift in Cu emission is governed by increased substitutionally doped dopant ions which creates hybridized states below CB edge.[22,40] Furthermore, after annealing, the percentage contribution of Cu emission increases from 88.2 and 99.4 to ~100 % for both acetate and nitrate-based samples respectively. This shift in dopant emission contribution is consistent with the degree of red-shift in dopant emission for both the cases. Although annealing helps to achieve full dopant emission, longer-time annealing at these temperatures is found to degrade the excitonic features of NPLs (Figure S22). Therefore, collective optimization of the experimental parameters with respect to the annealing temperature, time and environment may help to further increase the absolute PL QY of these doped-NPLs.

The spectral tunability of the Cu-induced emission in these doped NPLs was also investigated through the synthesis of Cu-doped NPLs having varying vertical thicknesses including 3 and 5 MLs via the versatile partial CE technique (see experimental section in the supporting information). Figure 6 exhibits the absorption and PL emission spectra of all our doped NPLs. As seen from the figure, it is conveniently possible to tune the Cu(I)-related emission in the doped NPL ensembles from 640 to 830 nm.

Finally, temperature-dependent PL decay dynamics in the doped-NPL ensemble were also examined for the exemplary case of 1.7 % Cu doping. Figure 7a shows the PL decay curves in the temperature range of 30–270 K. As the temperature was progressively decreased, we observed that the PL decay of the dopant emission slows down. As shown in Figure 7b, both amplitude-averaged lifetime and the longest lifetime component increase with

the decreasing temperature toward cryogenic temperatures. Below 60 K, a monotonic increase of the PL lifetime can be observed, which has previously been similarly reported for the Cu(I)-doped CdSe, InP and $CuInS_2$ CQDs.[36] This temperature- dependent increase in the lifetime for these NCs has been recently attributed to a magnetic-exchange splitting within the luminescent excited state.[36] A more detailed investigation of the temperature-dependent emission kinetics in these Cu(I) doped NPLs will also be of interest to the community to understand deeper into the photo-physics of these materials.

Discussion

The presented systematic and detailed studies of Cu(I) doping in the CdSe NPLs through the partial CE method provide a comprehensive understanding of the doping mechanism in these strongly confined quantum systems. Firstly, the 1+ oxidation state of Cu-dopant ions in the host core-only CdSe NPLs as confirmed by our XPS experiments was corroborated along with optical studies. Secondly, the careful control of the partial CE reactions and annealing of the non-uniform doped samples have resulted in almost 100% dopant induced PL emission. As discussed in the literature for Cu(I)-doped CdSe CQDs, Cu in 1+ oxidation state fundamentally cannot show any BE recombination. The photo-excited holes in the host CdSe are captured by Cu(I) ions, which in turn recombine with delocalized electrons of CB leading to dominant Stokes-shifted dopant induced PL emission. Therefore, these atomically-flat NPLs exhibit similar PL emission mechanism as in the case of Cu(I)-doped CQDs. The only appearing difference is, due to the large lateral area of the NPLs, the requirement of further experimental procedures to be controllable for achieving full Cu-based emission. Therefore, this study in general allows us to control and understand the evolution of dopant-related emission in strong QC regimes.

In the last decade, for these Cu-doped CdSe CQDs, apart from their unique optical and electronic properties, there has been a tremendous interest in the scientific community for understanding chemical dopant-induced hybridization of the host CdSe orbitals. In the past, tuning the bandgap (changing both VB and CB) with the size variation and alloying of CQDs was readily achievable.[45,46] However, controlling the position of individual VB/CB edges of CQDs with respect to photocathode/anode is needed for their practical applications in future CQD based devices.[22] Meulenberg et al. have shown in the past few years that increasing the amount of Cu(I)-dopant ions in the host CdSe CQDs affects the lowest empty electronic states (CB) in a way inconsistent with the quantum confinement (QC) theory.[40] Concisely, increasing Cu(I)-dopant ions in CdSe CQDs results in the decrease of CB edge (only), which further shifts the PL emission spectrum to longer wavelengths. Meulenberg et al. have explained these results as a result of the hybridization of CdSe orbitals by successful substitution of Cu(I) ions in the CdSe host medium proved this hypothesis through theoretical modelling, X-ray absorption (XAS) spectroscopy[40] and, more recently, ultraviolet photoemission spectroscopy (UPS).[22] However, presence of these electronically and optically active states below the CB due to Cu(I) doping and redshifting of emission spectra by increasing the number of dopant ions in the host lattice can be confused with the particle size distribution inherent within the ensemble of doped CdSe CQDs. To this end, strongly confined quasi-2D NPLs may serve as better systems to test these interesting theoretical and experimental observations. Here, the excitonic structure is mostly invariable due to the lateral size of the NPLs and the emission is originating from vertically confined direction, which is fixed for these NPLs. Therefore, any increase in Cu(I) doping at substitutional sites in CdSe NPLs should result in a redshift of the emission spectrum (and vice versa) according to this hybridization theory. In our detailed partial CE experiments, the consistent redshift of PL emission spectra with increasing doping strongly supports the hybridization of CB edge states

in the host CdSe NPLs. Figures 2c, 2f, 4d-4f and Figures S14-S16 show the systematic variation of the dopant emission peak wavelength with the increasing incorporation of Cu(I) ions in NPLs. Additionally, use of the same core for doping with different amounts of Cu(I) via the partial CE method provides an outstanding set of samples for understanding chemical dopant induced orbital hybridization model. Furthermore, the appearance of Cu(I)-related emission spectra with smaller energies than bandgap in excitation-dependent PL emission spectroscopy and the depth profile XPS results also confirm successful doping of Cu(I) in the host CdSe NPLs (see the supporting information, Figure S23, Table S2 and Sections E, F for detailed discussion).

In conclusion, we have carried out an elaborative and systematic study on the Cu(I) doping process in strongly 1D-confined CdSe NPLs possessing exceptional optical properties including the tunable PL emission in the visible-to-NIR spectral region and large Stokes shift accompanied with high PL QYs and large absorption cross-sections compared to doped CQDs. Here detailed XPS, steady-state PL and temperature-dependent time-resolved fluorescence spectroscopy investigations verified the successful Cu(I) doping in CdSe NPLs via the partial CE method proposed and developed for NPLs for the first time in this study. In this work, the slow doping of Cu(I) in CdSe uniquely allowed to develop a deep understanding of the photo-physics of dopant emission in strong QC regimes. The combination of stable and dominant dopant-related PL emission having minimum self-absorption along with significantly unchanging PL QYs at higher optical densities confirmed the advantages of successful doping of Cu(I) in CdSe NPLs. This simple yet powerful technique, together with the understanding of doping process, enable the controlled Cu(I) doping in NPLs, which could be extended to different transition metal elements for the next-generation optoelectronic and color conversion devices.

Experimental Section

Synthesis of 4 ML Thick CdSe Nanoplatelets- For a typical synthesis, 340 mg of cadmium myristate, 24 mg of Se, and 30 mL of ODE were loaded into a 100 mL three-neck flask. The solution was degassed and stirred at 95 °C under vacuum for an hour to evaporate volatile solvents and dissolve the cadmium myristate completely. Then, the heater was set to 240 °C and the vacuum was broken at 100 °C and the flask was filled with argon gas. As the temperature reached 195 °C, the color of the solution become yellowish and at this stage 120 mg of cadmium acetate dihydrate was introduced swiftly into the reaction. After the growth of CdSe NPLs at 240 °C for around 10 min, 1 mL of OA was injected and the temperature of the solution was decreased to room temperature using a water bath. The solution was centrifuged for 5 min at 6000 rpm and the supernatant was removed into another centrifuge tube. After adding of ethanol into the supernatant solution until it became turbid, the solution was centrifuged again at 6000 rpm for 10 min, and then the precipitates were dissolved and stored in toluene. The synthesis of 3 and 5 ML CdSe core NPLs is given in the supporting information.

Partial Cation-Exchange- All exchange reactions were carried out in an oxygen- and water-free glove box. CdSe NPL dispersion having 2.68×10^{-6} mol/L concentration was kept under stirring at 60 °C. For a typical partial cation-exchange reaction, 1 mL of above CdSe NPL dispersion was diluted to 4 mL in toluene. First dopant precursor was prepared by mixing 1 mL of 0.4 M ethanolic solution of $Cu(OAc)_2$ with 1.5 mL TOP. It was kept under stirring for 30 min at 45 °C. Similarly, the second dopant precursor is prepared by mixing 1 mL of 0.1 M ethanolic solution of Cu $(NO_3)_2$ with 1.5 mL of TOP in 30 min at 45 °C. It has been shown for QDs that TOP, being a soft base, binds to Cu(II) (intermediate soft acid), reducing the reactivity of dopant ions towards Se of CdSe NCs, which avoids full conversion of CdSe to

Cu_2Se phases.[2,20] Ethanol present in the solution was thus used to extract replaced Cd (II) ions in the NPLs. Different amounts of dopant precursors were prepared to achieve different doping concentrations. However, the total volume of the cationic solution was kept the same for each reaction with the addition of a premixed solution of TOP (3 vol%) and ethanol (2 vol%) for maintaining a fixed concentration of TOP and ethanol in all reactions. Using 50, 100, 150, 200, 250 μL of the stock solution with 1 mL of CdSe NPL dispersion (6.7×10^{-7} mol/L) leads to 0.5, 0.9, 1.7, 3.2 and 3.6% ((Cu/Cu+Cd)%) doping of Cu(I) in 4 ML CdSe NPLs. Similarly, 20, 40, 60, 80, 100, 120, 140, 160 μL of the stock solution of Cu $(NO_3)_2$ added in 1 mL of CdSe NPL dispersion (6.7×10^{-7} mol/L) resulted in 0.2, 0.4, 0.9, 1.2, 1.7, 2.5, 2.8 and 3.2% ((Cu/Cu+Cd)%) doping of Cu (I) in 4 ML CdSe NPLs. A similar method was followed for doping of 3 and 5 ML CdSe NPLs.

After adding the dopant precursor the samples were stirred vigorously and the solution was allowed to equilibrate while stirring for 1 h. After the completion of reaction, all the samples were precipitated with excess ethanol and washed several times using excess ethanol and dispersed in toluene and kept on stirring at 50 °C. Absorption and photoluminescence spectra were measured at different time intervals (1-9 days) to study the effect of doping these thin NPLs.

TRF Spectroscopy- Time-resolved fluorescence (TRF) spectroscopy measurements were performed by using a time-correlated single photon-counting (TCSPC) system (PicoQuant FluoTime 200, PicoHarp 300). We used the picosecond pulsed laser (PicoQuant) at 375 nm for excitation, and the laser intensity was kept low (~1 nJ/cm^2) so that the number of photogenerated excitons per NPL was much less than 1 ($\langle N \rangle \ll 1$). In addition, the TRF spectroscopy measurements at cryogenic temperatures were carried out using a closed-cycle He cryostat that is coupled with our TRF spectroscopy system. The measurements at room temperature were conducted in solution form of NPL samples using quartz cuvette, whereas

the measurements at cryogenic temperatures were carried out in their solid film forms on Si substrates using drop-casted samples. To analyze the photoluminescence decay curves, the photoluminescence decay curves were fitted with multi-exponential functions using FluoFit software in reconvolution mode.

In our low temperature TRF measurements, the pressure of the sample environment was ~0.0045 mmHg and, according to our calculations, the boiling point of TOP under this pressure is ~283 K. In addition, we intentionally increased the temperature up to 330 K under vacuum and then decreased it to cryogenic temperatures. Therefore, the possible inconsistency in the emission kinetics of the NPLs due to the differences in TOP amount was eliminated by allowing the complete evaporation of TOP under low pressure conditions. In the light of this information, we could obtain the TRF decays without the interference of the effects of TOP and at low temperatures ranging from 270 to 17 K, which is shown in Figure 7.

References

(1) Khan, A. H.; Dalui, A.; Mukherjee, S.; Segre, C. U.; Sarma, D. D.; Acharya, S. Efficient Solid-State Light-Emitting CuCdS Nanocrystals Synthesized in Air. *Angew. Chemie Int. Ed.* **2015**, *54*, 2643–2648.

(2) Sahu, A.; Kang, M. S.; Kompch, A.; Notthoff, C.; Wills, A. W.; Deng, D.; Winterer, M.; Frisbie, C. D.; Norris, D. J. Electronic Impurity Doping in CdSe Nanocrystals. *Nano Lett.* **2012**, *12*, 2587–2594.

(3) Yang, L.; Knowles, K. E.; Gopalan, A.; Hughes, K. E.; James, M. C.; Gamelin, D. R. One-Pot Synthesis of Monodisperse Colloidal Copper-Doped CdSe Nanocrystals Mediated by Ligand-Copper Interactions. *Chem. Mater.* **2016**, *28*, 7375–7384.

(4) Srivastava, B. B.; Jana, S.; Pradhan, N. Doping Cu in Semiconductor Nanocrystals: Some Old and Some New Physical Insights. *J. Am. Chem. Soc.* **2011**, *133*, 1007–1015.

(5) Stouwdam, J. W.; Janssen, R. A. J. Electroluminescent Cu-Doped CdS Quantum Dots. *Adv. Mater.* **2009**, *21*, 2916–2920.

(6) Viswanatha, R.; Brovelli, S.; Pandey, A.; Crooker, S. A.; Klimov, V. I. Copper-Doped Inverted Core/shell Nanocrystals With "permanent" optically Active Holes. *Nano Lett.* **2011**, *11*, 4753–4758.

(7) Wang, X.; Yan, X.; Li, W.; Sun, K. Doped Quantum Dots for White-Light-Emitting Diodes Without Reabsorption of Multiphase Phosphors. *Adv. Mater.* **2012**, *24*, 2742–2747.

(8) Yu, J. H.; Liu, X.; Kweon, K. E.; Joo, J.; Park, J.; Ko, K.-T.; Lee, D. W.; Shen, S.; Tivakornsasithorn, K.; Son, J. S.; *et al.* Giant Zeeman Splitting in Nucleation-Controlled Doped CdSe:Mn2+ Quantum Nanoribbons. *Nat. Mater.* **2010**, *9*, 47–53.

(9) Jawaid, A. M.; Chattopadhyay, S.; Wink, D. J.; Page, L. E.; Snee, P. T. Cluster-Seeded Synthesis of Doped CdSe:Cu4 Quantum Dots. *ACS Nano* **2013**, *7*, 3190–3197.

(10) Meulenberg, R. W.; van Buuren, T.; Hanif, K. M.; Willey, T. M.; Strouse, G. F.; Terminello, L. J. Structure and Composition of Cu-Doped CdSe Nanocrystals Using Soft X-Ray Absorption Spectroscopy. *Nano Lett.* **2004**, *4*, 2277–2285.

(11) Li, Z.; Peng, X. Size/shape-Controlled Synthesis of Colloidal CdSe Quantum Disks: Ligand and Temperature Effects. *J. Am. Chem. Soc.* **2011**, *133*, 6578–6586.

(12) Chen, D.; Gao, Y.; Chen, Y.; Ren, Y.; Peng, X. Structure Identification of Two-Dimensional Colloidal Semiconductor Nanocrystals with Atomic Flat Basal Planes. *Nano Lett.* **2015**, *15*, 4477–4482.

(13) Thoma, S. G.; Sanchez, A.; Provencio, P. P.; Abrams, B. L.; Wilcoxon, J. P. Synthesis, Optical Properties, and Growth Mechanism of Blue-Emitting CdSe Nanorods. *J. Am. Chem. Soc.* **2005**, *127*, 7611–7614.

(14) Boldt, K.; Kirkwood, N.; Beane, G. A.; Mulvaney, P. Synthesis of Highly Luminescent and Photo-Stable, Graded Shell CdSe/Cd xZn1-xS Nanoparticles by in Situ Alloying. *Chem. Mater.* **2013**, *25*, 4731–4738.

(15) Saunders, A. E.; Shieh, F.; Korgel, B. A. General Shape Control of Colloidal Cds, Cdse and Cdte Semiconductor Nanorods and Nanorod Heterostructures. In *AIChE Annual Meeting, Conference Proceedings*; 2005; p. 4640.

(16) White, S. L.; Smith, J. G.; Behl, M.; Jain, P. K. Co-Operativity in a Nanocrystalline Solid-State Transition. *Nat. Commun.* **2013**, *4*, 2933.

(17) Beberwyck, B. J.; Surendranath, Y.; Alivisatos, A. P. Cation Exchange: A Versatile Tool for Nanomaterials Synthesis. *J. Phys. Chem. C* **2013**, *117*, 19759–19770.

(18) Lesnyak, V.; Brescia, R.; Messina, G. C.; Manna, L. Cu Vacancies Boost Cation Exchange Reactions in Copper Selenide Nanocrystals. *J. Am. Chem. Soc.* **2015**, *137*, 9315− 9323.

(19) Bouet, C.; Laufer, D.; Mahler, B.; Nadal, B.; Heuclin, H.; Pedetti, S.; Patriarche, G.; Dubertret, B. Synthesis of Zinc and Lead Chalcogenide Core and Core/shell Nanoplatelets Using Sequential Cation Exchange Reactions. *Chem. Mater.* **2014**, *26*, 3002–3008.

(20) Gopal, M. B. Ag and Cu Doped Colloidal CdSe Nanocrystals: Partial Cation Exchange and Luminescence. *Mater. Res. Express* **2015**, *2*, 085004.

(21) De Trizio, L.; Prato, M.; Genovese, A.; Casu, A.; Povia, M.; Simonutti, R.; Alcocer, M. J. P.; D'Andrea, C.; Tassone, F.; Manna, L. Strongly Fluorescent Quaternary Cu-In-Zn-S Nanocrystals Prepared from Cu 1-xInS 2 Nanocrystals by Partial Cation Exchange. *Chem. Mater.* **2012**, *24*, 2400–2406.

(22) Wright, J. T.; Forsythe, K.; Hutchins, J.; Meulenberg, R. W. Implications of Orbital Hybridization on the Electronic Properties of Doped Quantum Dots: The Case of Cu:CdSe. *Nanoscale* **2016**, *8*, 9417–9424.

(23) Ithurria, S.; Dubertret, B. Quasi 2D Colloidal CdSe Platelets with Thicknesses Controlled at the Atomic Level. *J. Am. Chem. Soc.* **2008**, *130*, 16504–16505.

(24) Ithurria, S.; Tessier, M. D.; Mahler, B.; Lobo, R. P. S. M.; Dubertret, B.; Efros, A. L. Colloidal Nanoplatelets with Two-Dimensional Electronic Structure. *Nat. Mater.* **2011**, *10*, 936–941.

(25) Kelestemur, Y.; Guzelturk, B.; Erdem, O.; Olutas, M.; Gungor, K.; Demir, H. V. Platelet-in-Box Colloidal Quantum Wells: CdSe/CdS@CdS Core/Crown@Shell Heteronanoplatelets. *Adv. Funct. Mater.* **2016**, *26*, 3570–3579.

(26) Olutas, M.; Guzelturk, B.; Kelestemur, Y.; Yeltik, A.; Delikanli, S.; Demir, H. V. Lateral Size-

Dependent Spontaneous and Stimulated Emission Properties in Colloidal CdSe Nanoplatelets. *ACS Nano* **2015**, *9*, 5041–5050.

(27) Yeltik, A.; Delikanli, S.; Olutas, M.; Kelestemur, Y.; Guzelturk, B.; Demir, H. V. Experimental Determination of the Absorption Cross-Section and Molar Extinction Coefficient of Colloidal CdSe Nanoplatelets. *J. Phys. Chem. C* **2015**, *119*, 26768−26775.

(28) Guzelturk, B.; Kelestemur, Y.; Olutas, M.; Delikanli, S.; Demir, H. V. Amplified Spontaneous Emission and Lasing in Colloidal Nanoplatelets. *ACS Nano* **2014**, *8*, 6599–6605.

(29) She, C.; Fedin, I.; Dolzhnikov, D. S.; Dahlberg, P. D.; Engel, G. S.; Schaller, R. D.; Talapin, D. V. Red , Yellow , Green , and Blue Amplified Spontaneous Emission and Lasing Using Colloidal CdSe Nanoplatelets. *ACS Nano* **2015**, *9*, 9475–9485.

(30) Wang, Y.; Zhukovskyi, M.; Tongying, P.; Tian, Y.; Kuno, M. Synthesis of Ultrathin and Thickness-Controlled Cu 2– X Se Nanosheets via Cation Exchange. *J. Phys. Chem. Lett.* **2014**, *5*, 3608–3613.

(31) Izquierdo, E.; Robin, A.; Keuleyan, S.; Lequeux, N.; Lhuillier, E.; Ithurria, S. Strongly Confined HgTe 2D Nanoplatelets as Narrow Near-Infrared Emitters. *J. Am. Chem. Soc.* **2016**, *138*, 10496–10501.

(32) Sharma, M.; Gungor, K.; Yeltik, A.; Olutas, M.; Guzelturk, B.; Kelestemur, Y.; Erdem, T.; Delikanli, S.; McBride, J. R.; Demir, H. V. Near-Unity Emitting Copper-Doped Colloidal Semiconductor Quantum Wells for Luminescent Solar Concentrators. *Adv. Mater.* **2017**, *29*, 1700821.

(33) Knowles, K. E.; Hartstein, K. H.; Kilburn, T. B.; Marchioro, A.; Nelson, H. D.; Whitham, P. J.; Gamelin, D. R. Luminescent Colloidal Semiconductor Nanocrystals Containing Copper: Synthesis, Photophysics, and Applications. *Chem. Rev.* **2016**, *116*, 10820–10851.

(34) Whitham, P. J.; Knowles, K. E.; Reid, P. J.; Gamelin, D. R. Photoluminescence Blinking and Reversible Electron Trapping in Copper-Doped CdSe Nanocrystals. *Nano Lett.* **2015**, *15*, 4045–4051.

(35) Grandhi, G. K.; Viswanatha, R. Tunable Infrared Phosphors Using Cu Doping in Semiconductor Nanocrystals: Surface Electronic Structure Evaluation. *J. Phys. Chem. Lett.* **2013**, *4*, 409–415.

(36) Knowles, K. E.; Nelson, H. D.; Kilburn, T. B.; Gamelin, D. R. Singlet–Triplet Splittings in the Luminescent Excited States of Colloidal Cu+:CdSe, Cu+:InP, and CuInS2 Nanocrystals: Charge-Transfer Configurations and Self-Trapped Excitons. *J. Am. Chem. Soc.* **2015**, *137*, 13138–13147.

(37) Tang, A.; Yi, L.; Han, W.; Teng, F.; Wang, Y.; Hou, Y.; Gao, M. Synthesis, Optical Properties, and Superlattice Structure of Cu(I)-Doped CdS Nanocrystals. *Appl. Phys. Lett.* **2010**, *97*, 033112.

(38) Pandey, A.; Brovelli, S.; Viswanatha, R.; Li, L.; Pietryga, J. M.; Klimov, V. I.; Crooker, S. A. Long-Lived Photoinduced Magnetization in Copper-Doped ZnSe–CdSe Core–shell Nanocrystals. *Nat. Nanotechnol.* **2012**, *7*, 792–797.

(39) Hazarika, A.; Layek, A.; De, S.; Nag, A.; Debnath, S.; Mahadevan, P.; Chowdhury, A.; Sarma, D. D. Ultranarrow and Widely Tunable Mn2+-Induced Photoluminescence from Single Mn-Doped Nanocrystals of ZnS-CdS Alloys. *Phys. Rev. Lett.* **2013**, *110*, 267401.

(40) Wright, J. T.; Meulenberg, R. W. Effects of Dopants on the Band Structure of Quantum Dots: A Theoretical and Experimental Study. *Phys. Rev. B* **2013**, *88*, 45432.

(41) Nelson, H. D.; Li, X.; Gamelin, D. R. Computational Studies of the Electronic Structure S of Copper-Doped CdSe Nanocrystals: Oxidation States, Jahn-Teller Distortions, Vibronic Bandshapes, and Singlet-Triplet Splittings. *J. Phys. Chem. C* **2016**, *120*, 5714–5723.

(42) Radi, A.; Pradhan, D.; Sohn, Y.; Leung, K. T. Nanoscale Shape and Size Control of Cubic,

Cuboctahedral, and Octahedral Cu-Cu2O Core-Shell Nanoparticles on Si(100) by One-Step, Templateless, Capping-Agent-Free Electrodeposition. *ACS Nano* **2010**, *4*, 1553–1560.

(43) Mahler, B.; Guillemot, L.; Bossard-Giannesini, L.; Ithurria, S.; Pierucci, D.; Ouerghi, A.; Patriarche, G.; Benbalagh, R.; Lacaze, E.; Rochet, F.; *et al.* Metallic Functionalization of CdSe 2D Nanoplatelets and Its Impact on Electronic Transport. *J. Phys. Chem. C* **2016**, *120*, 12351–12361.

(44) Katari, J. E. B.; Colvin, V. L.; Alivisatos, A. P. X-Ray Photoelectron Spectroscopy of CdSe Nanocrystals with Applications to Studies of the Nanocrystal Surface. *J. Phys. Chem.* **1994**, *98*, 4109–4117.

(45) Murray, C. B.; Norris, D. J.; Bawendi, M. G. Synthesis and Characterization of Nearly Monodisperse CdE (E = S, Se, Te) Semiconductor Nanocrystallites. *J. Am. Chem. Soc.* **1993**, *115*, 8706–8715.

(46) Bailey, R. E.; Nie, S. Alloyed Semiconductor Quantum Dots: Tuning the Optical Properties without Changing the Particle Size. *J. Am. Chem. Soc.* **2003**, *125*, 7100–7106.

Acknowledgement

We gratefully acknowledge the financial support from the National Research Foundation of Singapore under its Investigatorship program (NRF-NRFI2016-08). HVD also acknowledges TUBA.

Additional Information

The Supporting Information is available free of charge on the ACS Publications website at DOI:

Additional UV-visible absorption, steady-state excitation and emission analysis, structural and elemental analyses which include additional HAADF based EDS images, XRD, HRTEM, XPS analyses, additional results for partial CE experiments, excitation wavelength dependent PL emission studies, XPS depth profile studies, effect of using TOP in doped NPLs and control sample (undoped NPLs), additional materials and methods (PDF).

Competing financial interests

The authors declare no competing financial interest.

Figures

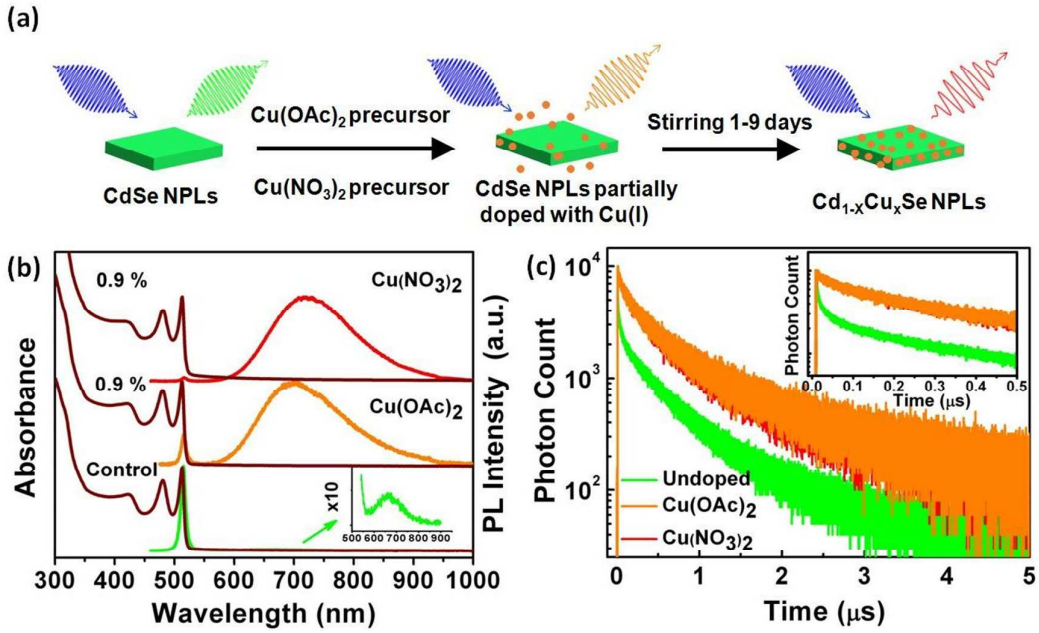

Figure 1. (a) Copper doping through partial cation exchange reaction by using copper-acetate and copper-nitrate precursors. (b) UV-visible absorption and normalized photoluminescence spectra, (c) room-temperature time-resolved fluorescence decay curves for undoped and 0.9% Cu-doped 4 ML CdSe NPLs synthesized using copper-acetate and copper-nitrate precursors. Inset in (b) shows the 10 times magnified view of weak defect emission for the case of undoped NPLs.

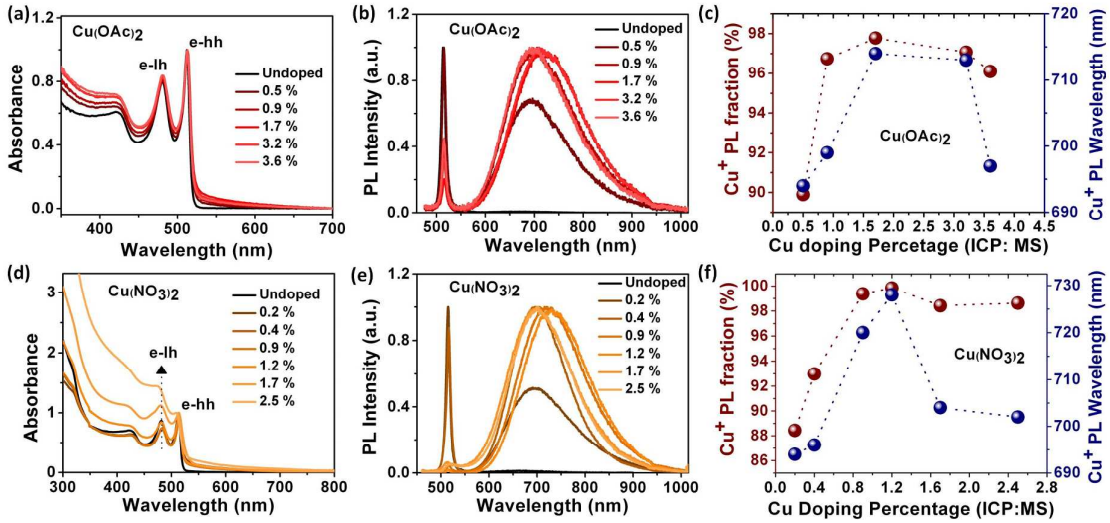

Figure 2.UV-visible absorption spectra and steady-state photoluminescence emission spectra of Cu(I)-doped CdSe NPLs, (a, b) using copper (II) acetate, (d, e) using copper (II) nitrate trihydrate precursors, (c, f) variation of I_{dopant}/I_{total} emission (Cu^{+} PL fraction) and peak emission wavelength with increasing Cu(I) to Cd(II) values for both series synthesized by acetate and nitrate precursors of copper, respectively.

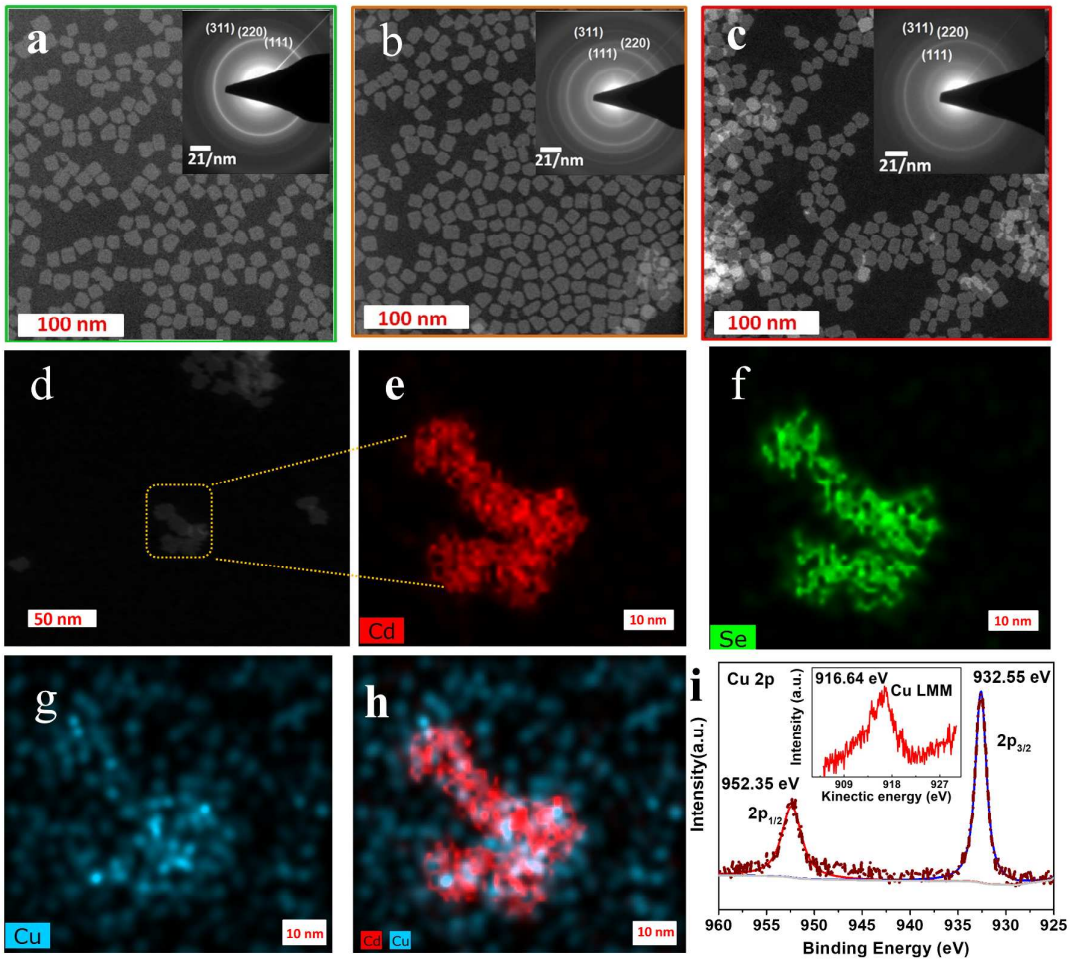

Figure 3. (a, b) HAADF-TEM images of (a) undoped and (b, c) 0.9% of Cu-doped NPLs using acetate and nitrate precursors. Inset of Figure 3 (a, c) shows SAED pattern for the corresponding samples, (d) HAADF-STEM images of 3.6% of Cu-doped 4 ML CdSe NPLs, (e-g) EDS maps of cadmium, selenium and copper, (h) overlaid EDS map of cadmium and copper. (i) High-resolution XPS spectra of Cu (2p) orbitals. Figure 3i (inset) shows Auger spectra of Cu LMM orbitals.

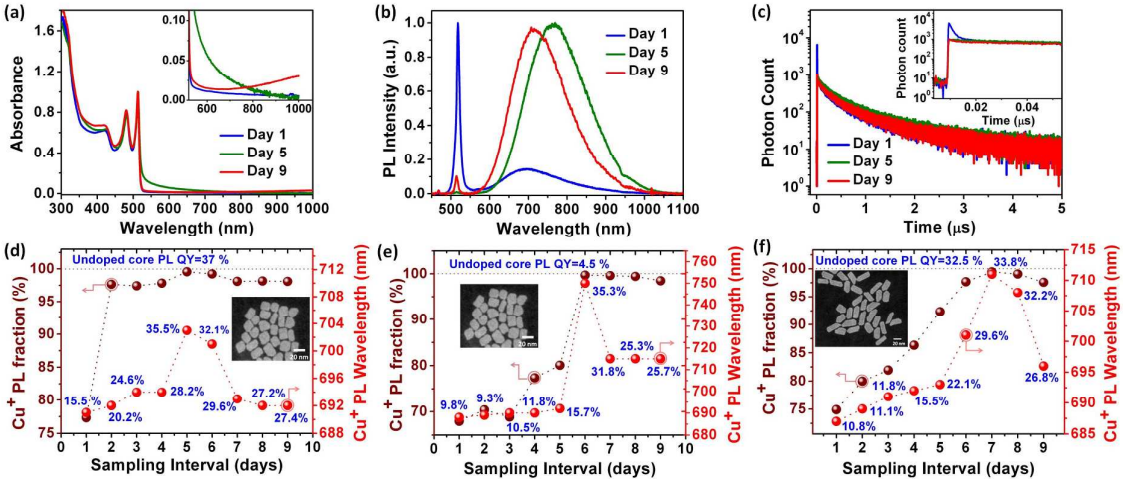

Figure 4. Mechanism of doping: (a-c) UV-visible absorption, steady-state emission and TRF decays for Cu-doped CdSe NPLs on different days of partial CE synthesis, (d-f) Variation of I_{dopant}/I_{total} emission (Cu^+ PL fraction) and peak emission wavelength with time for three different samples doped under identical conditions. Lateral area of samples in (d) and (e) is the same with each other i.e. 170.3 nm^2; however, the initial PL QYs of their core NPLs are different. Lateral area of NPLs given in (f) is 366.6 nm^2. Scale bars in all inset TEM micrographs are 20 nm.

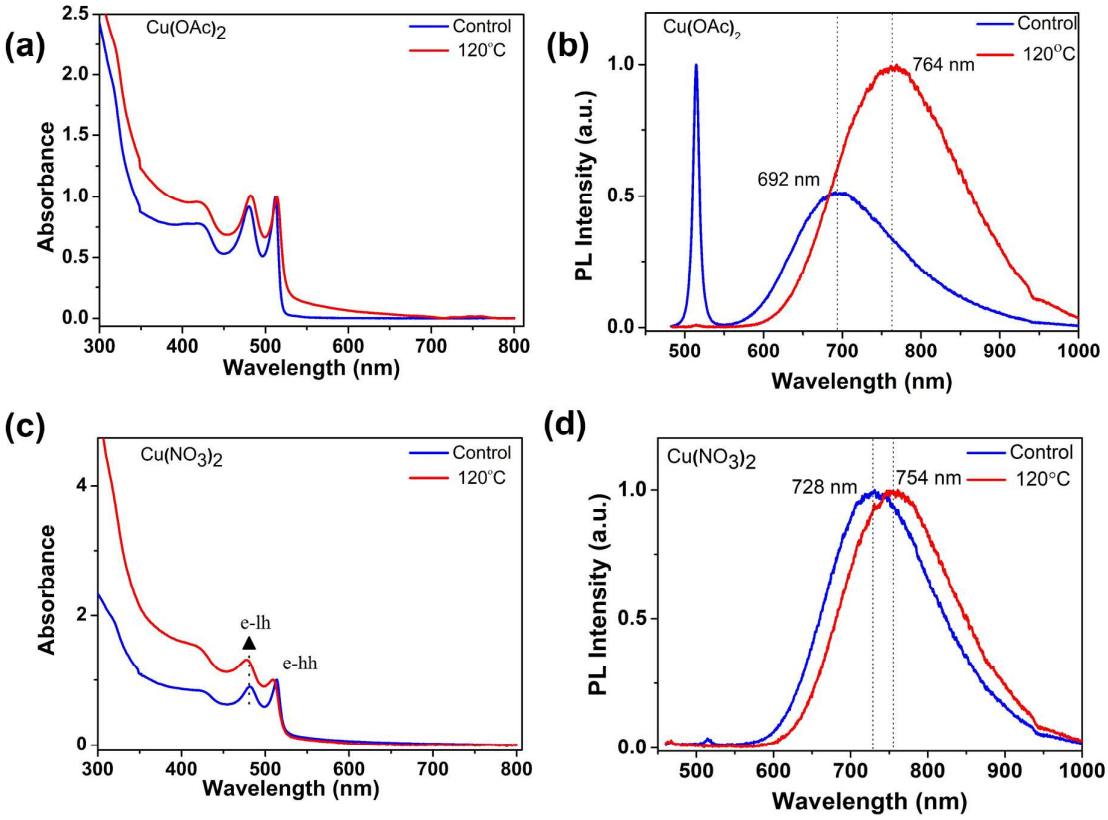

Figure 5. (a-d) UV-visible absorption and PL emission spectra of Cu-doped CdSe NPLs annealed at 120 °C for 30 min in nitrogen filled glove box.

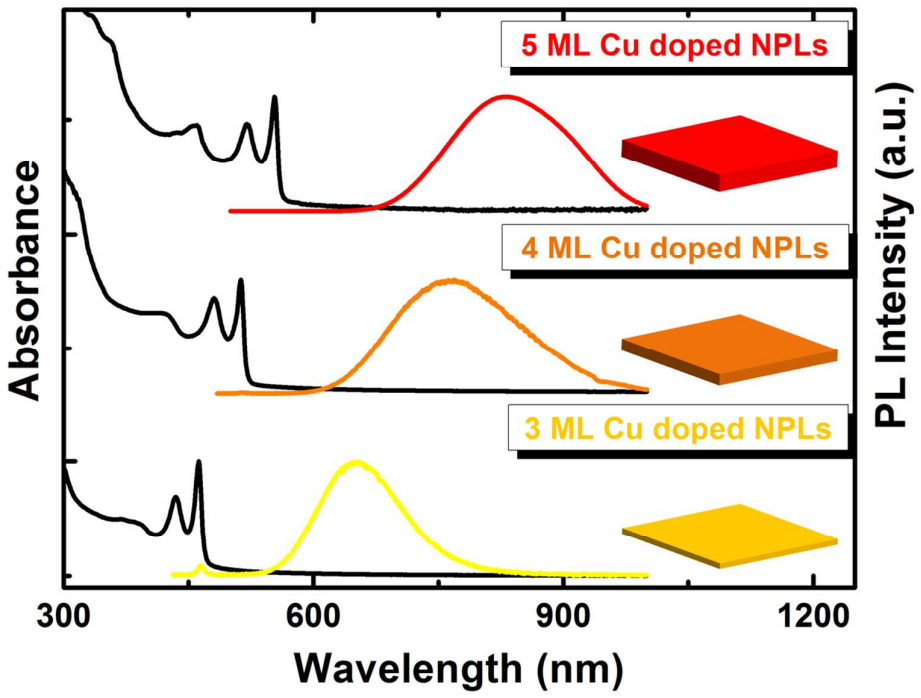

Figure 6. UV absorption and PL emission spectra of (a) 3 ML (yellow), 4 ML (orange) and 5 ML (red) Cu-doped CdSe NPLs. The highest PL QYs for the 3-5 ML Cu-doped NPLs are 28, 63 and 51 %, respectively.

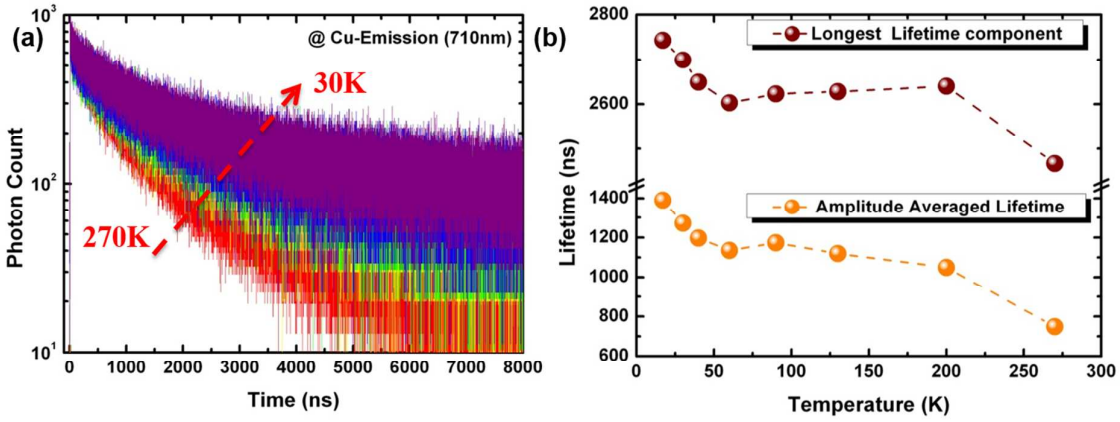

Figure 7. (a) The PL decay profile of Cu-emission in CdSe NPLs at different cryogenic temperatures (red @270 K and violet @30 K), (b) amplitude-averaged and longest lifetimes for Cu-doped NPLs as a function of the measurement temperature ranging from 270 to 17 K.

TOC Figure

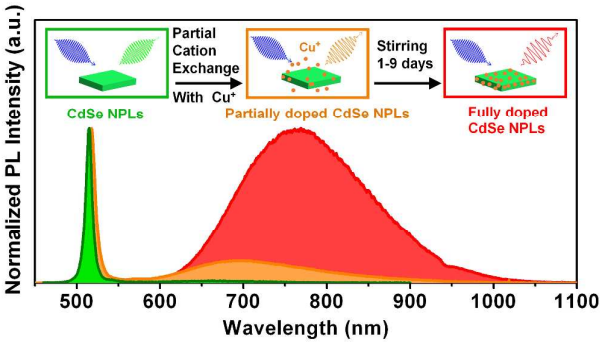
Partial
Cation
Exchange
With Cu+
Cu+
Stirring
1-9 days
CdSe NPLs
Partially doped CdSe NPLs
Fully doped
CdSe NPLs
Normalized PL Intensity (a.u.)
500
600
700
800
900
1000
1100
Wavelength (nm)